Stark Interference of Electric and Magnetic Dipole Transitions in the $A - X$ Band of OH

H. Christian Schewe, Dongdong Zhang,* and Gerard Meijer†
Fritz-Haber-Institut der Max-Planck-Gesellschaft, Faradayweg 4-6, D-14195 Berlin, Germany

Robert W. Field
Department of Chemistry, Massachusetts Institute of Technology, Cambridge, Massachusetts 02139, USA

Boris G. Sartakov
General Physics Institute, RAS, Vavilov Street 38, 119991 Moscow, Russia

Gerrit C. Groenenboom and Ad van der Avoird§
Theoretical Chemistry, IMM, Radboud University, Heyendaalseweg 135, 6525 AJ Nijmegen, The Netherlands

Nicolas Vanhaecke‡
Fritz-Haber-Institut der Max-Planck-Gesellschaft, Faradayweg 4-6, D-14195 Berlin, Germany
and Laboratoire Aimé Cotton, CNRS, Université Paris-Sud, ENS Cachan, Université Paris-Saclay, 91405 Orsay, France
(Received 6 February 2016; published 11 April 2016)

An experimental method is demonstrated that allows determination of the ratio between the electric ($E1$) and magnetic ($M1$) transition dipole moments in the $A - X$ band of OH, including their relative sign. Although the transition strengths differ by more than 3 orders of magnitude, the measured $M1$-to-$E1$ ratio agrees with the ratio of the *ab initio* calculated values to within 3%. The relative sign is found to be negative, also in agreement with theory.

DOI: 10.1103/PhysRevLett.116.153001

In atoms and molecules, higher order transitions, such as magnetic dipole allowed transitions ($M1$) or electric quadrupole allowed transitions ($E2$) are typically between 5 and 7 orders of magnitude weaker than the corresponding electric dipole allowed transitions ($E1$). However, in some atomic or molecular species where the $E1$ transitions are rather weak, the $M1$-to-$E1$ ratio can become relatively large, up to the order of 10^{-3} [1,2]. This has great influence on experiments relying on quantitative measurements of quantum state populations that require very sensitive state-selective detection, for instance, in fully state-resolved collision experiments [3]. Currently, great effort is undertaken to realize laser cooling of molecules [4] and to implement magneto-optical traps for molecules [5,6]. These laser-cooling schemes rely on electric dipole selection rules to rotationally and vibrationally close the laser-cooling cycles [7]. However, if $M1$ transitions are less probable than $E1$ transitions by only a factor of $\approx 10^{-3}$–10^{-4}, these must be considered as possible loss channels.

In this Letter, we present a general experimental method employing interference between the transition dipole moments to measure the ratio of the strengths of $M1$ and $E1$ transitions. By applying a static electric and a static magnetic field in a controlled manner, the amplitudes of the magnetic and electric dipole transitions are mixed at comparable intensity into one signal. This method resembles the Stark-interference technique in atomic spectroscopy [8–10] and has so far been applied only once to a molecular system for radio frequency transitions [11]. Also the relative sign of the $E1$ and $M1$ transition dipole moments can be determined by this interference technique. We demonstrate its application to electronic transitions in a molecular system by measuring the $M1$-to-$E1$ ratio in the A–X band of OH on individually resolved hyperfine-state transitions. We reproduce the ratio between accurate *ab initio* calculated values of the $E1$ and $M1$ transition dipole moments [2] to better than 3%, and the relative sign agrees with the *ab initio* calculations. The method is generally applicable to other transitions in OH as well as to many other molecular systems.

The $X^2\Pi$ ground state of the OH radical with total angular momentum $J = 3/2$ consists of a Λ doublet with components e and f corresponding to parities $p = -1$ and $+1$, respectively. The energy splitting between the doublet states is 1680 MHz. The ^{16}O nucleus has spin zero and the H nucleus has spin $I = 1/2$. When hyperfine interactions are taken into account, each of the doublet states splits into a hyperfine triplet with $F = 1$ and quintet with $F = 2$. The $F = 2$ levels are higher in energy than the $F = 1$ levels by 53 and 55 MHz for the e and f states, respectively. The lowest excited electronic state is the $A^2\Sigma^+$ state with parity $p' = +1$ in its rotational ground state with $J' = 1/2$. It is split by hyperfine interactions into $F' = 0$ and $F' = 1$ levels separated in energy by 778 MHz. A qualitative level scheme is shown in the upper part of Fig. 1. Electric dipole transitions to the $A^2\Sigma^+, J' = 1/2, p' = +1$ state are allowed from the $X^2\Pi, J = 3/2e$ state with $p = -1$ and

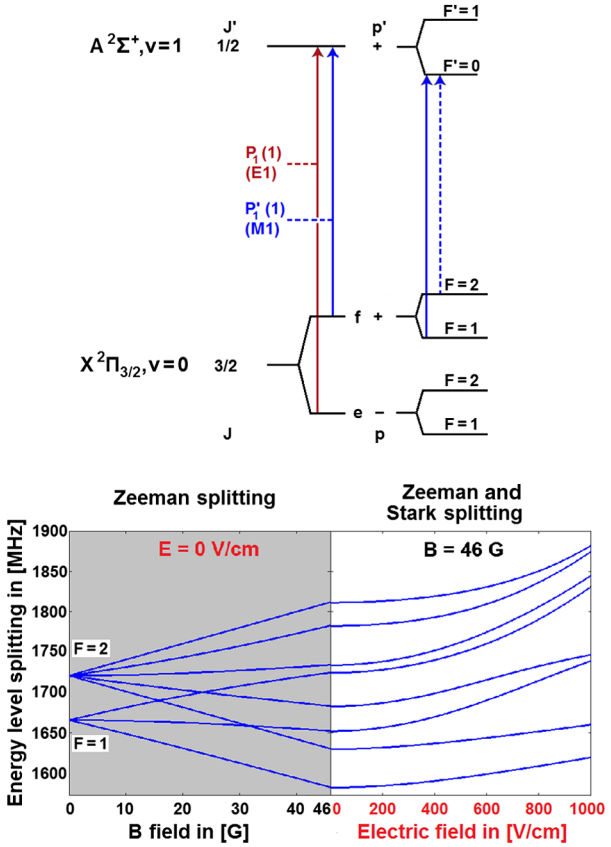

FIG. 1. The upper drawing shows the ground ($X^2\Pi_{3/2}, v = 0$) and excited ($A^2\Sigma^+, v' = 1$) states and the electric and magnetic dipole transitions investigated. The bottom picture shows the eight split energy levels (blue curves) of the upper Λ-doublet component of the ground state in perpendicular static electric and magnetic fields.

magnetic dipole transitions from the $X^2\Pi, J = 3/2f$ state with $p = +1$. The transitions measured start from the vibrational $v = 0$ level of the $X^2\Pi, J = 3/2$ ground state and end in the $v' = 1$ level of the $A^2\Sigma^+, J' = 1/2$ excited state. The corresponding vibronic transition dipole moments are given by

$$\langle \Pi_{\pm 1}|\mu^{\mathrm{el}}_{\pm 1}|\Sigma\rangle \quad \text{and} \quad \langle \Pi_{\pm 1}|\mu^{\mathrm{mag}}_{\pm 1}|\Sigma\rangle, \tag{1}$$

where $|\Pi_{\pm 1}\rangle$ denotes the spherical components of the $X^2\Pi, v = 0$ wave function, $|\Sigma\rangle$ is the $A^2\Sigma^+, v' = 1$ wave function, and $\mu^{\mathrm{el}}_{\pm 1}$ and $\mu^{\mathrm{mag}}_{\pm 1}$ are the spherical components of the electric and magnetic dipole operators. The relations between spherical tensor components and Cartesian components are given in Ref. [12]. All components are defined with respect to a molecule-fixed frame with its z axis pointing from the O to the H nucleus. The permanent electric dipole moment is positive. The magnetic dipole moment is related to the electronic orbital angular momentum and spin operators $\mathbf{L}$ and $\mathbf{S}$ as $\boldsymbol{\mu}^{\mathrm{mag}} = -\mu_B(\mathbf{L} + g_e\mathbf{S})/\hbar$, where $\mu_B = e\hbar/(2m_e)$ is the Bohr magneton, $\hbar$ the reduced Planck constant, m_e the electron mass, $g_e = 2.0023$, and the minus sign occurs because electrons have a negative charge. The spin operator $\mathbf{S}$ does not contribute to the perpendicular transition from the $X^2\Pi$ state to the $A^2\Sigma^+$ state. The Cartesian transition matrix elements $\langle \Pi_y|\mu^{\mathrm{el}}_y|\Sigma\rangle = -0.05249ea_0$ and $\langle \Pi_y|L_x|\Sigma\rangle = -0.2834i\hbar$ were calculated *ab initio* [2]. The wave function $|\Pi_y\rangle$ denotes a Cartesian component of the $X^2\Pi, v = 0$ state. The signs of the wave functions are arbitrary, but since we used the same wave functions for both matrix elements, the relative sign of the transition moments is well defined. The spherical electric and magnetic transition dipole matrix elements are $\langle \Pi_{+1}|\mu^{\mathrm{el}}_{+1}|\Sigma\rangle = -0.05249ea_0$ and $\langle \Pi_{+1}|\mu^{\mathrm{mag}}_{+1}|\Sigma\rangle = 0.2834\mu_B$. Both are real valued and their relative sign is negative.

Stark interference occurs when the $A \leftarrow X$ transitions are measured in the presence of external static electric and magnetic fields $\mathbf{E}_{\mathrm{stat}}$ and $\mathbf{B}_{\mathrm{stat}}$. The Hamiltonian of the field-free OH radical is invariant under inversion and under time reversal. Inversion symmetry is broken by the external electric field $\mathbf{E}_{\mathrm{stat}}$, which causes mixing of the Λ-doublet states $|X^2\Pi, -\rangle$ and $|X^2\Pi, +\rangle$ with parities $p = -1$ and $p = +1$, respectively. The upper $p = +1$ state obtains a contribution from the lower $p = -1$ state and its wave function becomes $(|X^2\Pi, +\rangle + \delta|X^2\Pi, -\rangle)/\sqrt{1+\delta^2}$. The mixing parameter δ is small and proportional to E_{stat} as long as the Stark energy is small compared to the energy gap between the Λ-doublet levels. Such mixing hardly occurs for the upper $A^2\Sigma^+$ state with parity $p' = +1$, because it is separated from the next state with $p' = -1$ by a rotational energy gap of about 35 cm^{-1}. The mixed initial $X^2\Pi$ state is coupled to the final $A^2\Sigma^+$ state by both the electric and magnetic dipole operators, and the transition line strength becomes

$$\begin{aligned}\mathcal{L} &= |(\langle X^2\Pi, +| + \delta\langle X^2\Pi, -|)(\mathbf{E}\cdot\boldsymbol{\mu}^{\mathrm{el}} + \mathbf{B}\cdot\boldsymbol{\mu}^{\mathrm{mag}})|A^2\Sigma, +\rangle|^2/(1+\delta^2)\\ &= (|\langle X^2\Pi, +|\mathbf{B}\cdot\boldsymbol{\mu}^{\mathrm{mag}}|A^2\Sigma, +\rangle|^2 + \delta^2|\langle X^2\Pi, -|\mathbf{E}\cdot\boldsymbol{\mu}^{\mathrm{el}}|A^2\Sigma, +\rangle|^2\\ &\quad + 2\delta\mathrm{Re}[\langle X^2\Pi, -|\mathbf{E}\cdot\boldsymbol{\mu}^{\mathrm{el}}|A^2\Sigma, +\rangle\langle X^2\Pi, +|\mathbf{B}\cdot\boldsymbol{\mu}^{\mathrm{mag}}|A^2\Sigma, +\rangle])/(1+\delta^2).\end{aligned} \tag{2}$$

The symbols $\mathbf{E}$ and $\mathbf{B} = \mathbf{k}\times\mathbf{E}/c$ denote the laser electric and magnetic field polarization vectors, $\mathbf{k}$ is a unit vector in the laser propagation direction, c is the speed of light, and $\mathrm{Re}[\cdots]$ indicates that one should take the real part of the expression in square brackets. The last term in Eq. (2) containing the product of the electric and magnetic transition dipole moments is due to Stark interference between the electric and magnetic dipole transitions.

Hyperfine states with total angular momentum $F = 1$ and $F = 2$ become mixed by the static electric field, so that F is no longer a good quantum number. The projection M_F on the direction of $\mathbf{E}_{\text{stat}}$ remains a good quantum number.

Stark interference cannot be observed, however, when only an external electric field is present. The reason is that the electric field breaks parity, but does not break time-reversal symmetry. Levels with opposite values of the magnetic quantum number M (the hyperfine levels with $M_F = \pm 1$ and $M_F = \pm 2$ in this case) are interconverted by time reversal and remain degenerate. The magnetic transition dipole moment changes sign under time reversal, and since one has to average the line strength over degenerate initial states, the net effect is that the interference term cancels by averaging over the degenerate states with opposite M_F values. When a static magnetic field is also applied, time-reversal symmetry is broken and the degeneracy of the levels with opposite values of M_F is lifted by Zeeman splitting. If the laser has sufficient resolution to resolve this splitting, Stark interference can actually be observed. When the two external static fields are parallel M_F remains a good quantum number, but this is not essential. The external magnetic field does not break parity; hence, the mixing between states of opposite parity by the static electric field is not affected by the additional magnetic field.

Figure 1 illustrates the above theory. The upper scheme depicts the transitions between the rovibronic ground state $|X^2\Pi_{3/2}, v = 0, J = 3/2\rangle$ and the lowest excited state $|A^2\Sigma^+, v' = 1, J' = 1/2\rangle$ of OH. The hyperfine levels are indicated by their quantum numbers $F = 1$ and $F = 2$ in the ground state and $F' = 0$ and $F' = 1$ in the excited state. Transitions from $F = 2$ to $F' = 0$ are forbidden, but become allowed when external fields are applied and F is no longer a good quantum number. The spectroscopic investigations address the $M1$ transition $P_1'(1)$ $(A^2\Sigma^+,\ v' = 1,\ J' = 1/2,\ p' = +1 \leftarrow X^2\Pi_{3/2}, v = 0,$ $J = 3/2f, p = +1)$ and the $E1$ transition $P_1(1)$ $(A^2\Sigma^+,$ $v' = 1,\ J' = 1/2,\ p' = +1 \leftarrow X^2\Pi_{3/2},\ v = 0,\ J = 3/2e,$ $p = -1)$, which are indicated by blue and red arrows, respectively. The lower part of Fig. 1 shows the hyperfine levels with $F = 1$ and $F = 2$ of the upper Λ-doublet component of the $X^2\Pi, J = 3/2$ ground state and their combined Zeeman and Stark splittings as a function of the external static magnetic and electric fields. The mixing of the different parity components of the ground state wave function by the static electric field allows the electric transition dipole moment to contribute to the transitions from these initial levels, which under field-free conditions is purely driven by the magnetic transition dipole moment.

In the experiment a magnetic field $\mathbf{B}_{\text{stat}}$ is applied perpendicular to both the electric field $\mathbf{E}_{\text{stat}}$ and the propagation direction $\mathbf{k}$ of the detection laser. The laser polarization is aligned such that the polarization directions $\mathbf{E}$ and $\mathbf{B}$ make an angle of 45° with $\mathbf{E}_{\text{stat}}$ and $\mathbf{B}_{\text{stat}}$. The interference term has the property to reverse sign if either $\mathbf{k}$ or one of the static fields $\mathbf{E}_{\text{stat}}$ and $\mathbf{B}_{\text{stat}}$ is reversed. This causes the same transition to have a different intensity. When only the electric field $\mathbf{E}_{\text{stat}}$ is applied, the intensity depends quadratically on the field strength for weak fields and has its minimum at $E_{\text{stat}} = 0$. At this minimum the intensity equals the pure $M1$ contribution. When the magnetic field $\mathbf{B}_{\text{stat}}$ is applied simultaneously, the intensity distribution is no longer symmetric with respect to $E_{\text{stat}} = 0$. When the Stark interference is destructive, the intensity of a transition becomes smaller than the corresponding pure $M1$ contribution.

A schematic overview of the experimental setup is shown in Fig. 2. Samples of state-selected and velocity-controlled OH molecules are produced using a pulsed supersonic molecular beam source combined with a Stark decelerator [13]. For the present spectroscopic experiments, quantum-state selected samples of OH molecules containing both low-field seeking Stark components ($\Omega M_J = -3/4$ and $-9/4$) of the ground state $|X^2\Pi_{3/2}, v = 0, J = 3/2, f\rangle$ are prepared with a translational velocity of 625 m/s. A bunching scheme is applied to minimize the transverse velocity spread of the OH packet [14], resulting in a residual Doppler broadening of each transition of less than 5 MHz. After leaving the Stark decelerator, the molecules enter the detection chamber

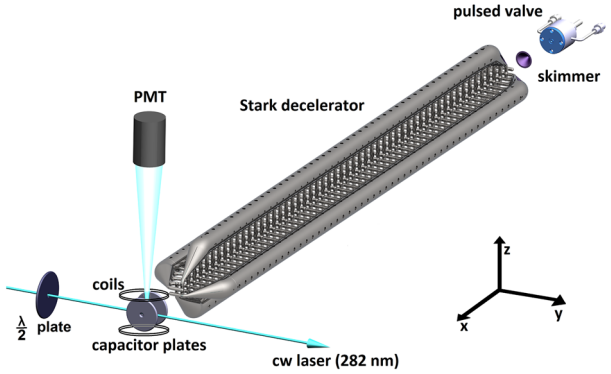

FIG. 2. Scheme of the experimental setup. The translational axis of the decelerator defines the x axis and the cw laser propagation direction is aligned along the y axis. Two capacitor plates with a diameter of 44 mm are mounted at 25 mm from each other, symmetrically with respect to the center of the detection zone. Each plate has a hole with a diameter of 4 mm through which the OH beam enters the detection region. Voltages are applied to the plates to create a homogeneous static electric field $\mathbf{E}_{\text{stat}}$ parallel to the x axis. Two coils of copper wire with a diameter of 60 mm are also mounted symmetrically at a distance of 32 mm, to create a homogeneous static magnetic field $\mathbf{B}_{\text{stat}}$ along the z axis. The field strengths E_{stat} and B_{stat} are tuned by the voltages and the currents applied, and the fields are reversed by reversing the polarity of the voltage or the direction of the applied current. The field distributions of $\mathbf{E}_{\text{stat}}$ and $\mathbf{B}_{\text{stat}}$ are calibrated and simulated to determine the actual field strengths and field configurations and to evaluate systematic errors. This shows that both fields are known with an accuracy of 1%.

through an aperture in a metallic shield, which serves as a differential pumping stage. It also shields the detection zone from all residual electric fields from the Stark decelerator. After a flight distance of 6.25 cm, the molecules arrive in the center of the detection chamber, where the spectroscopic investigations are performed.

The OH radicals are detected via laser-induced fluorescence with a continuous wave ring dye laser system (Coherent 899-21) that is actively stabilized. The dye-laser radiation is frequency doubled in an external cavity, where typically a power of 4 mW is obtained with a bandwidth of ± 2 MHz. The laser propagation direction $\mathbf{k}$ is determined by the SHG setup to be horizontal along the y axis. A $\lambda/2$ plate is used to rotate $\mathbf{E}$ manually over any desired angle within an accuracy of 0.5°. Transitions are induced in the $A^2\Sigma^+, v' = 1 \leftarrow X^2\Pi_{3/2}, v = 0$ band near 282 nm. Fluorescent photons from the $A^2\Sigma^+, v' = 1 \rightarrow X^2\Pi_{3/2}, v = 1$ band around 314 nm are collected vertically along the z axis by a lens and collimated onto a photomultiplier tube (PMT). Stray light is suppressed by light baffles and by optical filtering in front of the PMT. Single photons are detected and counted. At each frequency the number of photons is averaged over a series of measurements at constant E_{stat} and B_{stat}. Long-term drifts are eliminated by changing the values of E_{stat} and B_{stat} in random order and repeating the measurements. The laser power is recorded permanently to normalize the counted number of photons at each data point.

Both parts of Fig. 3 depict the experimentally measured spectra as red solid curves. They are plotted as a function of the relative laser frequency for five different applied E_{stat} values: 0, ± 400, and ± 600 V/cm. The upper and lower pictures correspond to B_{stat} values of -30.0 and 46.0 G, respectively, applied throughout the measurements. The black solid curves show the best fits of calculated spectra to all experimental data. All line intensities fit very well as a function of the relative frequency and the asymmetries of the transitions as a function of the applied E_{stat} agree very well for all eight transitions. This fitting procedure is used to determine the ratio of the electric and magnetic transition dipole moments, as well as their relative sign.

In the fitting procedure, the population and the interfering $E1$ and $M1$ amplitudes of each of the eight transitions are modeled. The line intensities are described by Eq. (2) and multiplied with fit parameters that represent the initial state populations. The magnetic field has to be turned on 200 μs before the molecules arrive in the interaction zone for the sake of its temporal stability during the laser detection. This affects the rescrambling of the M_F states of the molecules after they leave the decelerator by an unknown amount, and, therefore, the eight initial state populations are used as independent fit parameters. The line profile is modeled by a Gaussian function in which the line width due to Doppler broadening is also a fit parameter. Furthermore, the electric field is influenced by the metallic coils. A small potential is needed for the current that creates $\mathbf{B}_{\text{stat}}$. This results in an angular offset of $\mathbf{E}_{\text{stat}}$ of 3° from the beam axis, which is included as well.

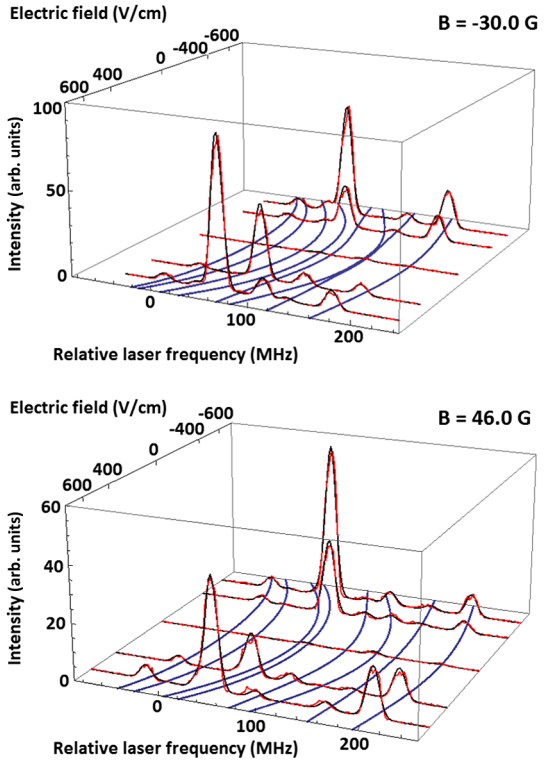

FIG. 3. Measured (red lines) and fitted (black lines) spectra as function of the static electric field strength E_{stat}, for two different static magnetic field values. The blue curves under each of the eight peaks indicate the calculated center frequencies of the transitions originating from each of the eight hyperfine levels in the ground state (shown in Fig. 1) to the single, nondegenerate $F' = 0$ hyperfine level in the excited state. The intensity is given in arbitrary units.

Table I lists the fit results for the sets of measurements depicted in Fig. 3. Additionally, it shows results from fitting a set of measurements in which $B_{\text{stat}} = 46.0$ G while the laser was propagating in the opposite direction ($-\mathbf{k}$). If we use the definition of the electric and magnetic transition dipole moments in Eq. (1) and define their dimensionless ratio r as

$$r = \frac{c\langle \Pi_{+1}|\mu_{+1}^{\text{el}}|\Sigma\rangle}{\langle \Pi_{+1}|\mu_{+1}^{\text{mag}}|\Sigma\rangle}, \tag{3}$$

TABLE I. Results of fits to three experimental data sets.

B_{stat} [G]	Laser direction	r from fit	Standard error	No. of measurements averaged
46.0	$\mathbf{k}$	-52.9	± 1.1	1000
-30.0	$\mathbf{k}$	-51.3	± 1.3	1000
46.0	$-\mathbf{k}$	-48.3	± 2.6	250

the *ab initio* calculated transition dipole moments [2] quoted above yield a value $r = -50.8$. The fit values of r from the experimental data agree with the theoretical value to within the standard error of the mean and they agree also for the relative sign of the two transition dipole moments. The *ab initio* calculated ratio is reproduced with an error of less than 3%, which is 10 times better than in previous measurements [2].

The experimental method presented here can be applied to other transitions in OH and to many other molecular systems. The hyperfine interactions that play a role in the present experiments on OH are not essential; the only requirements are that states of opposite parity are sufficiently close in energy to be mixed by a static electric field and that the Zeeman splitting between levels with opposite values of the magnetic quantum number M induced by a static magnetic field can be resolved.

[*]Present address: Department of Chemistry, University of Basel, Basel, Switzerland.
[†]Present address: Radboud University, Heyendaalseweg 135, 6525 AJ Nijmegen, Netherlands.
[‡]Present address: European Patent Office, Patentlaan 2, 2288 EE Rijswijk, Netherlands.
[§]Corresponding author.
A.vanderAvoird@theochem.ru.nl

[1] X. Yang and P. J. Dagdigian, J. Mol. Spectrosc. **198**, 189 (1999).
[2] M. Kirste, X. Wang, G. Meijer, K. B. Gubbels, A. van der Avoird, G. C. Groenenboom, and S. Y. T. van de Meerakker, J. Chem. Phys. **137**, 101102 (2012).
[3] M. Kirste, X. Wang, H. C. Schewe, G. Meijer, K. Liu, A. van der Avoird, L. M. C. Janssen, K. B. Gubbels, G. C. Groenenboom, and S. Y. T. van de Meerakker, Science **338**, 1060 (2012).
[4] E. S. Shuman, J. F. Barry, and D. DeMille, Nature (London) **467**, 820 (2010).
[5] M. T. Hummon, M. Yeo, B. K. Stuhl, A. L. Collopy, Y. Xia, and J. Ye, Phys. Rev. Lett. **110**, 143001 (2013).
[6] J. F. Barry, D. J. McCarron, E. B. Norrgard, M. H. Steinecker, and D. DeMille, Nature (London) **512**, 286 (2014).
[7] B. K. Stuhl, B. C. Sawyer, D. Wang, and J. Ye, Phys. Rev. Lett. **101**, 243002 (2008).
[8] M. A. Bouchiat and C. Bouchiat, J. Phys. (Paris) **36**, 493 (1975).
[9] S. L. Gilbert, R. N. Watts, and C. E. Wieman, Phys. Rev. A **29**, 137 (1984).
[10] C. S. Wood, S. C. Bennett, D. Cho, B. P. Masterson, J. L. Roberts, C. E. Tanner, and C. E. Wieman, Science **275**, 1759 (1997).
[11] W. M. Itano, Phys. Rev. A **22**, 1558 (1980).
[12] D. M. Brink and G. R. Satchler, *Angular Momentum*, 3rd ed. (Clarendon, Oxford, 1993).
[13] L. Scharfenberg, H. Haak, G. Meijer, and S. Y. T. van de Meerakker, Phys. Rev. A **79**, 023410 (2009).
[14] F. M. H. Crompvoets, R. T. Jongma, H. L. Bethlem, A. J. A. van Roij, and G. Meijer, Phys. Rev. Lett. **89**, 093004 (2002).